Skin Tone via Device-Independent Colour Space

Leah DeVos[1], Gennadi Saiko[2] [a] and Alexandre Douplik[2,3] [b]

[1]Department of Engineering, Toronto Metropolitan University, Toronto, Canada
[2]Department of Physics, Toronto Metropolitan University, Toronto, Canada
[3]iBest, Keenan Research Centre of the LKS Knowledge Institute, St. Michael's Hospital, Canada

Keywords: Skin Tone, Melanin, Tissue Optics.

Abstract: *Background:* Skin colour is essential to skin and wound assessment as it brings valuable information about skin physiology and pathology. An approach, which can help deconvolute and isolate various mechanisms affecting skin colour, could be helpful to drive the rPPG utility beyond its current applications. *Aim:* The present work aims to create a framework that links skin colour with melanin content. *Material and methods:* The model consists of two parts. First, the model's core connects tissue chromophore concentrations with changes in tissue reflectance. Seven-layer tissue models and Monte Carlo simulations were used to obtain the tissue reflectance spectra. In the second step, the tissue reflectance is convoluted with the responsivity of a sensor (tristimulus response in the case of the human eye) and the light source's emission spectrum. *Results:* The model allows linking melanin content with skin colour. *Conclusion:* The model can be helpful for the interpretation of the amplitudes of various components of the rPPG signal.

1 INTRODUCTION

Optical methods in the visible range have difficulties extracting physiological parameters in subjects with darker skin. Recent reporting identified potential skin tone biases of PPG. For instance, Sjoding et al. (Sjoding, 2020) investigated the occurrence of occult hypoxemia across patients who self-identified as White or Black, which is true oxygen saturation of <88% given a PPG-quantified saturation from 92-96% (i.e., a false negative from PPG on detection of low saturation). They reported that occult hypoxemia occurred in 12% of patients who self-identified as Black, compared to 4% of patients who self-identified as White.

Thus, it is plausible that current clinical datasets are skewed toward subjects with lighter skin complexion resulting in bias toward lighter skin tones. Consequently, the validity of the immense amount of accumulated clinical data may be questionable. Thus, the research on the influence of skin tone on optical physiological data (e.g., tissue oxygenation) and algorithms considering/correcting this impact are necessary.

Thus, the first step in this direction would be to establish quantifiable metrics. However, clinically used metrics (Fitzpatrick's skin tones) are subjective, and more objective models are required although to be correlated with the Fitzpatrick's scale to provide consistency of the 'results' interpretation.

Thus, the critical step in that direction is using objective (non-device specific) colour representation. RGB, by far, is the most common colour space; however, it suffers several drawbacks. The International Commission on Illumination (CIE) adopted the CIE XYZ colour space to overcome the disadvantages of trichromatic additive colour spaces like RGB. However, CIE XYZ space demonstrates perceptual nonuniformity (MacAdams, 1942). In adopting the CIELUV colour space, the CIE attempted to address this concern (Colorimetry, 1986).

In previous work (Saiko, 2022) the skin colour dependence on blood oxygenation and perfusion was studied analytically. In the current work we aim to investigate the influence of melanin content on skin colour using Monte Carlo simulations. Ultimately

[a] https://orcid.org/0000-0002-5697-7609
[b] https://orcid.org/0000-0001-9948-9472

this framework can help extract additional information from rPPG signals.

2 METHODS

The model conceptually consists of two parts. On step one we calculate the tissue reflectance. On step two we convolute the tissue reflectance with light source spectrum and sensor response curves (tristimulus response in the case of the human eye).

2.1 Tissue Reflectance

For this experiment, the spectrums of total and diffuse reflectance at various percentages of melanin content were simulated using the Monte Carlo method. To achieve this, first a layer model was designed to depict a computational model of human skin tissue. Then using that model, Monte Carlo simulations were run for the wavelength spectrum of 400-1000 nm with 5 nm increments, for melanin concentrations of 1, 2, 4, 6, 8, 16, and 32% respectively.

2.1.1 Tissue Model

The computational modelling of skin tissue is based on the consideration that skin is a three-dimensional half-infinite medium divided into several layers with varying optical properties (Wang, Jacques, & Zheng, 1995). The layers considered in this experiment are the stratum corneum, the living epidermis, the papillary dermis, the upper blood net dermis, the reticular dermis, the deep blood net dermis, and the subcutaneous fat. The top two layers (stratum corneum and living epidermis) comprises the bloodless epidermal layer. Stratum corneum is the first layer and is approximately 20 μm thick, it is

composed of flattened dead cells mainly containing keratin (Meglinsky & Matcher, 2001). The second layer is the living epidermis and is mainly composed of living cells including, dehydrated cells, laden cells with keratohyalin granules, columnar cells, melanin dust, small melanin granules and melanosomes (Meglinsky & Matcher, 2001). This layer is approx. 80 μm thick. The dermis has the inhomogeneous distribution of the blood vessels and skin capillaries within the skin (Meglinsky & Matcher, 2001). To emulate this complexity, we split the dermis layer into four sublayers, the papillary dermis (150 μm thick), the upper blood net dermis (80 μm thick), the reticular dermis (1500 μm thick) and the deep blood net dermis (170 μm thick). The last layer considered is the subcutaneous fat. We approximated it as 6 mm thick. The physical organisation of these layers can be visualised in Figure 1. Table 1 demonstrates the order of these layers as well as some of their optical and physical properties. The values for layer thickness and optical properties are an approximation and would vary slightly between in vivo subjects.
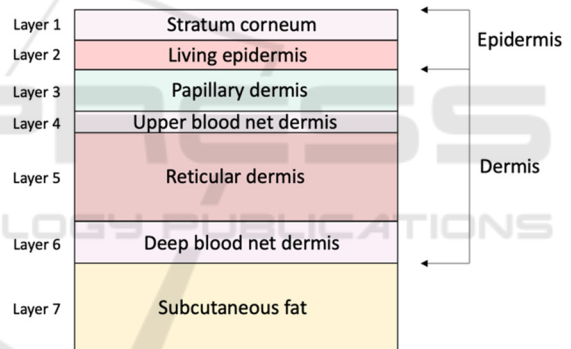

Figure 1: Skin layers for Monte Carlo simulations.

Table 1: Layer settings for $\lambda = 700$ nm and 1% melanin concentration, where n = refractive index, μ_a = absorption coefficient, μ_s = scattering coefficient, g = scattering anisotropy, d = layers thickness, C_b = blood volume fraction and C_w = water volume fraction.

#	Skin Layer	n	μ_a(cm^{-1})	μ_s(cm^{-1})	g	d (mm)	C_b	C_w
1	Stratum corneum	1.33	0.0012	285.71	0.9	0.02	0	0.2
2	Living epidermis	1.33	2.2162	285.71	0.85	0.05	0	0.2
3	Papillary dermis	1.37	0.0207	183.52	0.8	0.15	0.004	0.65
4	Upper blood net dermis	1.4	0.0881	183.52	0.9	0.08	0.02	0.65
5	Reticular dermis	1.4	0.0207	183.52	0.76	1.5	0.004	0.65
6	Deep blood net dermis	1.4	0.1723	183.52	0.95	0.17	0.04	0.65
7	Subcutaneous fat	1.44	0.1266	183.52	0.8	6	0.03	0.05

2.1.2 Optical Settings in Layer Model

The values of the optical properties set in this experiment were found both from existing literature as well as derived from optical equations. Retrieved from literature were the values for scattering anisotropy which was set to 0.9 and the values for the refractive index which ranged from around 1.34-1.53 depending on the tissue layer (Moço, Stuijk, & de Haan, 2018). This experiment ran simulations for a wavelength range of 400 to 1000 nm for each different concentration of melanin. For each wavelength and skin configuration the scattering and absorption coefficients for both the epidermal and the dermal layers was adjusted. The optical properties represented in Table 1 correspond to a wavelength of 700 nm and a concentration of melanin of 1%. The equations used to derive the values for the scattering and absorption coefficients of the dermis and epidermis were retrieved from work by Jacques et al (S. Jacques, T. Li & S. Prahl, 2019).

Absorption Coefficient, μ_a

The same equation is used to calculate the absorption coefficient of both the epidermis and the dermis, but the calculations differ in which input values were included or omitted. For example, when calculating the absorption coefficient of the epidermis, the volume fraction of melanosomes had to be considered while it did not for the absorption coefficient of the dermis and was set to zero. For the dermis, differing from the epidermis, in calculating the absorption coefficient, the average volume fraction of blood had to be included. The equation used to calculate the absorption coefficients was:

$$\mu_a = C_b(SO2\mu_{a.HbO2} + (1 - SO2)\mu_{a.RHb}) + \quad (1)$$
$$C_w\mu_{a.water} + C_m\mu_{a.melanosome} + C_f\mu_{a.fat}$$

Where: C_b = blood volume fraction, $SO2$ = oxygen saturation of hemoglobin, C_w = water volume fraction, C_f = fat volume fraction, Cm = volume fraction of melanosomes, $\mu_{a.HbO2}$ = absorption coefficient of oxygenated hemoglobin, $\mu_{a.RHb}$ = absorption coefficient of deoxygenated hemoglobin, $\mu_{a.fat}$ = absorption coefficient of fat, $\mu_{a.water}$ = absorption coefficient of water, and $\mu_{a.melanosome}$ = absorption coefficient of melanosomes.

Scattering Coefficient, μ_s

Tissue scattering is described as a summation of Rayleigh and Mie Scattering. To calculate the scattering coefficient first the reduced scattering coefficient, which describes the diffusion of photons

in a random walk, needs to be calculated. After the reduced scattering coefficient has been calculated, it can be incorporated with the anisotropy to calculate the scattering coefficient. The main difference between the scattering coefficient of the epidermis versus the dermis is that dermal scattering is described in terms of the relative contributions of Mie and Rayleigh scattering due to collagen fibres while epidermal scattering is relative to scattering due to keratin fibres (Jacques, 1998). Again, the same equations were used to calculate the scattering coefficient of the dermis and the epidermis differing only by the values of the input parameters. The equations used were as follows:

$$\mu_s' = \mu_{s.500}'(f_r\left(\frac{\lambda}{500}\right)^{-4} + (1 - f_m)\left(\frac{\lambda}{500}\right)^{-bm}) \quad (2)$$

$$\mu_s = \frac{\mu_s'}{1-g} \quad (3)$$

Where μ_s' = reduced scattering coefficient, μ_s = scattering coefficient, $\mu_{s.500}'$ = reduced scattering coefficient at 500 nm, f_r = fraction of Rayleigh scattering at 500 nm, f_m= fraction of Mie scattering at 500 nm, b_m = scatter power for Mie scattering, λ is the wavelength in [nm] and g is the anisotropy of scattering.

2.1.3 Monte Carlo Simulations of Skin Reflectance

For this experiment the Monte Carlo for Multi-Layered media (MCML) program by L. Wang & S. L. Jacques was used to provide a realistic model of light propagation in biological tissue (Wang & Jacques, 1992). In essence, the Monte Carlo method describes the transport of an infinitely narrow photon beam perpendicularly incident on a multi-layered tissue (Wang et al, 1995). Running Monte Carlo simulations generates a variety of output results but the output of interest for this experiment was the total and diffuse reflectance. To achieve these results, first an input file was generated to specify the simulation. This input file was generated in MATLAB using the function create_MCML_input_file that sets up the layer model used to describe the multi-layered tissue the simulation is being performed on (Akerstam & Andersson-Engels, 2011). An example of this layer model can be seen in Table 1. In the input file the number of incident photons to be used is also declared, for this experiment the amount of photons set was 100000. Once the input file has been generated, the input file is fed to the MCML program, and the simulation is run. Once the simulation is finished an output file is generated with the results. The MATLAB program getmcml.m was used to read

the generated output file and interpret the results (Wang & Jacques, 1992). These results include the diffuse and specular reflectance, which when combined provides the total reflectance. This process was repeated for a wavelength range of 400 to 1000 nm at different volume fractions of melanosomes. Using these results, the total reflectance and diffuse reflectance versus wavelength was plotted for each volume fraction of melanosomes of interest.

2.2 Light Source

It should be noted that while the colour representation for additive colour schemas (emissive case) can be considered absolute, it is not the case for subtractive colour schemas (reflection and transmission), where the response needs to be convoluted with the spectral power distribution of the illuminant. Thus, perceived colour in a subtractive colour scheme is light source dependent.

CIE standard illuminant E was used as the light source in our simulations.

2.3 Tristimulus Colour Space

The human eye and typical imaging systems interpret colours using three colour channels. Thus, in step 2, we need to aggregate the tissue reflectance spectra into three-channel responses. The CIE XYZ colour space encompasses all colour sensations visible to a person with average eyesight using the CIE's colour matching functions $(\overline{x}(\lambda), \overline{y}(\lambda), \overline{z}(\lambda))$, which quantify the chromatic response of the average observer. The CIE 1931 colour space defines the tristimulus values denoted by X, Y, and Z. In the case of the subtractive colour schema (reflection and transmission) for the known light source spectral distribution *I(l)*, the tristimulus values can be found as

$$X = \frac{K}{N} \int_{\lambda} R(\lambda) I(\lambda) \overline{x}(\lambda) d\lambda \qquad (4)$$

$$Y = \frac{K}{N} \int_{\lambda} R(\lambda) I(\lambda) \overline{y}(\lambda) d\lambda \qquad (5)$$

$$Z = \frac{K}{N} \int_{\lambda} R(\lambda) I(\lambda) \overline{z}(\lambda) d\lambda \qquad (6)$$

Here $N = \int_{\lambda} I(\lambda) \overline{y}(\lambda) d\lambda$, R is the tissue reflectance, and K is the scaling factor. The XYZ colour space can be transformed into commonly used RGB colour space by a simple linear transformation (multiplication on a 3x3 matrix).

However, the CIE XYZ colour space allows decomposition into two parts: brightness and

chromaticity. The CIE XYZ colour space was deliberately designed so that the *Y* parameter is also a measure of the luminance of a colour. That allows the representation of each colour on 2D colour space using normalization

$$x = \frac{X}{X + Y + Z} \qquad (7)$$

$$y = \frac{Y}{X + Y + Z} \qquad (8)$$

The chromatic coordinates (x,y) can be transformed into chromatic coordinates (u',v') in the CIELUV colour space (Colorimetry, 1986), which has certain advantages over the CIE XYZ colour space (namely, perceptual uniformity):

$$u' = \frac{4x}{-2x + 12y + 3} \qquad (9)$$

$$v' = \frac{9y}{-2x + 12y + 3} \qquad (10)$$

3 RESULTS

In the first step, we generated the tissue's simulated reflectance spectrum in the 400-1000 nm range for different melanin content (1, 2, 4, 6, 8, 16, and 32%, respectively). The results of the MC simulations are depicted in Figure 2.
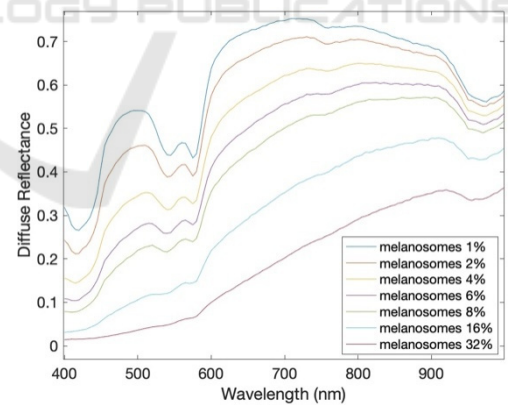

Figure 2: The skin diffuse reflectance spectrum as a function of the melanin content (1, 2, 4, 6, 8, 16, and 32%, respectively).

In step 2, the generated spectra were convoluted with CIE's colour matching functions and light source spectrum to obtain values X, Y, and Z using Eqs. 4-6. We approximated the CIE XYZ colour-matching functions by a sum of Gaussian functions (Wyman et al., 2013). CIE standard illuminant E was used as the light source.

Then using Eqs.7 and 8, x and y were obtained. The result of tissue colour simulations in (x,y) colour space is presented in Fig 3 as a function of the melanin content (1, 2, 4, 6, 8, 16, and 32%, respectively).
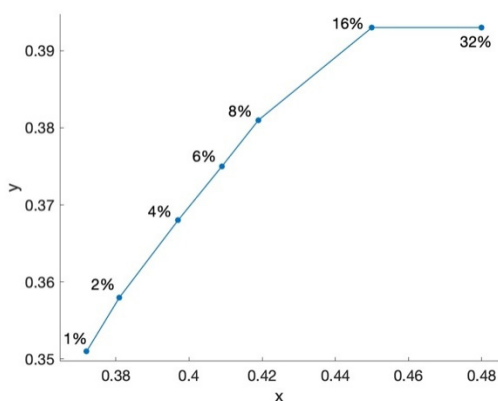

Figure 3: The simulated tissue colour in chromaticity diagrams (CIE XYZ colour space) as a function of the melanin content (1, 2, 4, 6, 8, 16, and 32%, respectively).

The respective transformation into CIELUV colour space using Eqs. 9-10 is depicted in Fig 4 as a function of the melanin content (1, 2, 4, 6, 8, 16, and 32%, respectively).
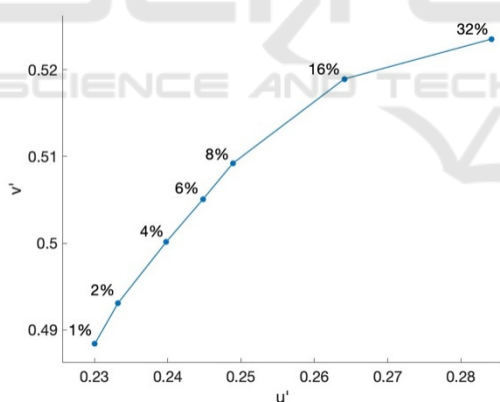

Figure 4: The simulated tissue colour in chromaticity diagrams (CIELUV colour space) as a function of the melanin content (1, 2, 4, 6, 8, 16, and 32%, respectively).

4 CONCLUSIONS

In summary, we proposed a simple approach where the realistic tissue reflectance spectrum generated using the multi-layer Monte Carlo model is onvoluted with CIE's colour-matching functions and ambient light spectrum to obtain tristimulus values in XYZ colour space. The proposed approach allows for quantitative analysis of the influence of tissue chromophores on tissue colour.

REFERENCES

Akerstam E. & Andersson-Engels S. (2011). "Monte Carlo Simulations of Light Transport in Tissue. Department of Physics, Lund University. https://www.atomic.physics.lu.se/fileadmin/atomfysik/Biophotonics/Education/Tissue_Optics_-_Computer_Exercise_-_MC.pdf

Colorimetry, 2nd ed, CIE publication 15.2, (Central Bureau CIE, Vienna, 1986)

Jacques S. (1998). "Skin Optics". Oregon Medical Laser Center News. https://omlc.org/news/jan98/skinoptics.html

Jacques S., Li T., & Prahl S. (2019). mcxyz.c. Monte Carlo Light Scattering Programs. https://omlc.org/software/mc/mcxyz/index.html

MacAdams D.L., (1942) Visual sensitivities to color differences in daylight. J OSA. 32(5) 247–274

Meglinsky, I. V., & Matcher, S. J. (2001). Modelling the sampling volume for skin blood oxygenation measurements. Medical & Biological Engineering & Computing, 39(1), 44-50. doi:10.1007/BF02345265

Moço, A. V., Stuijk, S., & de Haan, G. (2018). New insights into the origin of remote PPG signals in visible light and infrared. Scientific Reports, 8(1), 8501-15. doi:10.1038/s41598-018-26068-2

Saiko G (2022) How skin color depends on tissue oxygenation, Adv Exp Med Biol (submitted)

Sjoding, MW et al. (2020) Racial bias in pulse oximetry measurement. New England Journal of Medicine 383(25): 2477-2478

Wang L. & Jacques S. L. (1992). "(MCML) Monte Carlo for Multi-Layered media". Monte Carlo Light Scattering Programs. https://omlc.org/software/mc/

Wang, L., Jacques, S. L., & Zheng, L. (1995). MCML—Monte Carlo modeling of light transport in multi-layered tissues. Computer Methods and Programs in Biomedicine, 47(2), 131-146. doi:10.1016/0169-2607(95)01640-F

Wyman C; Sloan PP; Shirley P. (2013) Simple Analytic Approximations to the CIE XYZ Colour Matching Functions. J Comp Graph Tech. 2 (2): 1-11